

Clark County Desert Conservation Program (DCP)

Desert Tortoise Habitat Research

Draft v1.1

Final Project Report

Contract: 26-8274-8312 (BEG)

2009-UTX-811G (Clark County)

By

Kutalmis Saylam, John H. Andrews and Michael H. Young

Bureau of Economic Geology
John A. and Katherine G. Jackson School of Geosciences
The University of Texas at Austin

Principal Contacts

Kutalmis Saylam, kutalmis.saylam@beg.utexas.edu
Research Scientist Associate

Michael H. Young, michael.young@beg.utexas.edu
Senior Research Scientist, Associate Director

March 6, 2015

Contents

1) Introduction	3
2) Methods & Materials	5
a) Lidar Data Acquisition	5
b) Data Processing and Calibration	5
c) Vegetation Modeling	7
d) Geomorphic Features	10
e) Computation method	10
3) Results and Discussion	15
a) Digital Elevation Model	15
b) Field Measurements	16
c) Computational Findings	17
d) Other Features of Interest; Ledges and Stream Networks	20
4) Conclusion	23
Acknowledgements.....	24
Appendix A – Field vegetation measurement.....	25
Appendix B – C++ and AWK Code	26
References	32

1) Introduction

As part of the effort to protect desert tortoises and their habitats, the overall goal of this project was to analyze previously collected airborne data and to develop a fine-scale model to predict potential habitat locations of the endangered desert tortoise (*Gopherus agassizii*) in the Boulder City Desert Conversation Program (DCP) area and similar landscapes. The advanced analysis done herein will estimate vegetative cover, percent shade cover, and species richness of perennial and ephemeral plant species. These characteristics of this desert ecosystem could affect potential habitats for the desert tortoise.

This project extends research conducted previously by the Bureau of Economic Geology of the University of Texas at Austin. Specifically, in November 2013, the Bureau conducted an aerial Lidar and imagery survey in the DCP area in Eldorado Valley, south of the city of Boulder City, NV. The survey was conducted using the Chiroptera sensor (Airborne Hydrography AB, Jönköping, Sweden), at an approximate pulse rate of 100 - 150 kHz, varying with the flight altitude, flight speed, and project requirements. Location of the survey area was split into 4 blocks to better accommodate changing terrain elevation and repetition rate of the Lidar instrument. Resolution of data collection was 5-8 data points per square meter. Figure 1 presents the project location as captured by Landsat-8 satellite camera coinciding with the airborne survey date. The figure shows that DCP is split by U.S. Highway 95 into a north section (15,802 ha) and a south section (19,172 ha). A total of 1,040 hectares were designated by Boulder City for energy development (known as the Energy Zone), which were not analyzed in this study.

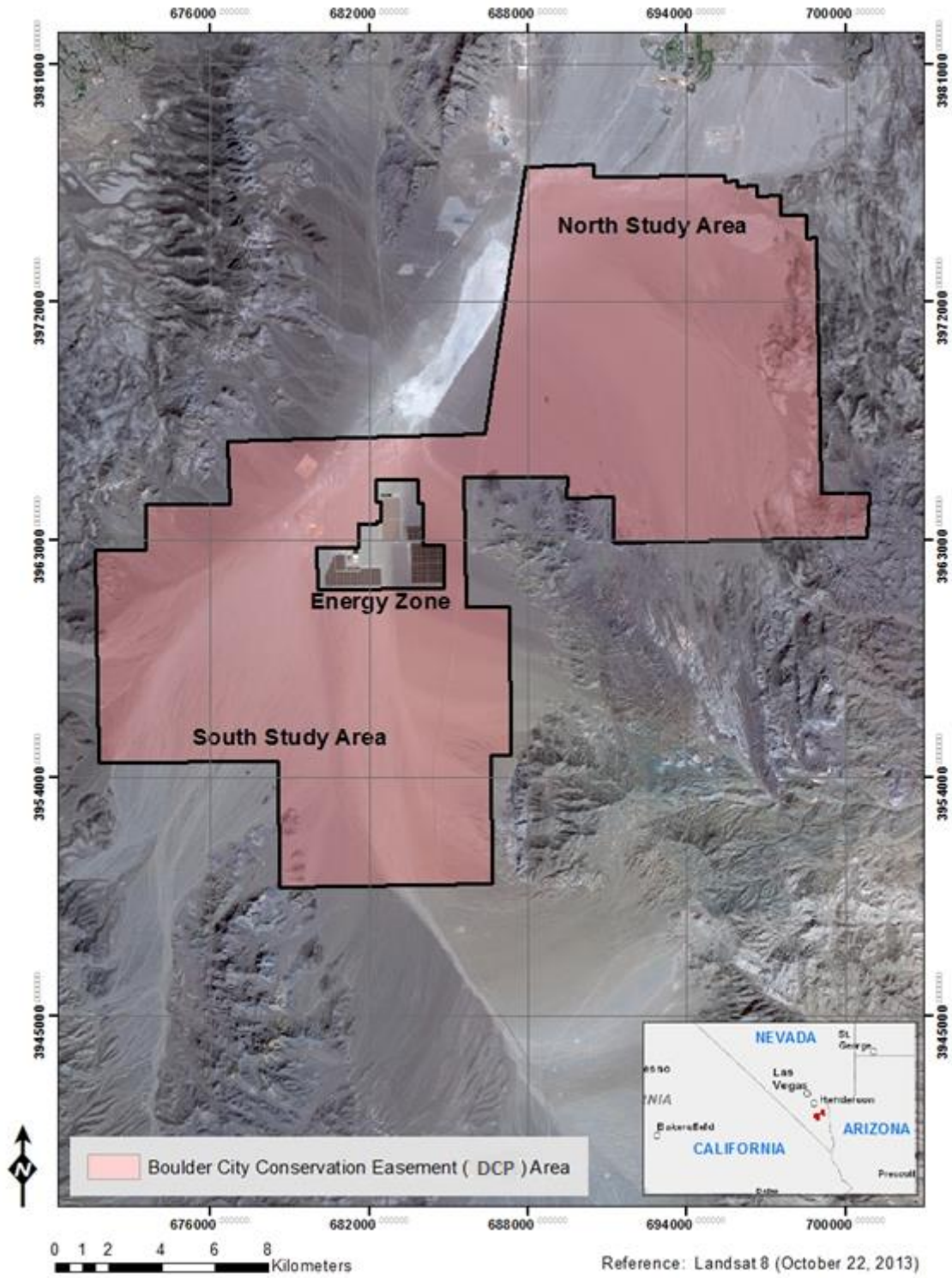


Figure 1: Project location overview map

2) Methods & Materials

a) Lidar Data Acquisition

During the original survey completed in 2013, a total of 3,366 raw images and approximately 4 billion Lidar points were captured in five separate Lidar flight missions, with a total of 88 linear flight lines. The Color infrared (CIR) imagery were captured and stored in proprietary Hasselblad format (3FR), which retained the details of the original image while reducing its size with a lossless compression. These raw images were converted into TIFF format and color balanced for optimum mosaic generation. Following image processing, however, we noted that some images taken during one of the surveys were not properly recorded due to hardware malfunction. Clark County representatives provided RGB imagery (TIFF) with 15cm resolution of these missing areas to assist with the analysis. Those images were acquired in early 2014; substantial changes to this ecosystem between the Bureau's image acquisition in late 2013 and Clark County's image acquisition in early 2014 were not expected to be significant, so we blended the two image sources into a single mosaic of imagery.

b) Data Processing and Calibration

AHAB's software Lidar Survey Suite v2.09 ("LSS") was used to convert raw laser files (.dat) into industry standard LAS (v1.2) file format. Terra Solid (TerraScan, v.014.28) application software was then used to merge individual segment files into individual flight lines. These flight lines were tiled into 226 individual 2,000 x 2,000 m tiles to ease the computation load for analyzing and storing the data. Tiles were named respectively accordingly to the southwestern point coordinates. All tiles were adjusted to real world elevation using an interpolated Geoid model 2012A provided by National Geodetic Survey¹.

Calibration of a Lidar system is a complex task, constructed by systematic procedures. The procedures include several steps beginning with in-situ measurements at the site followed by calculations with data processing algorithms. Corrections help to estimate system parameters for outputting the most accurate data that represents ground surface. Misalignments and poor calibration are mostly caused by using incorrect Inertial Navigation System (INS) rotation angles: roll, pitch and yaw (Ω , Φ , and K , respectively). Errors caused by pitch and roll misalignments can be detected by analyzing adjacent and overlapping Lidar strips. In theory, if no rotational misalignments are present, Lidar points registered in opposite flight directions should match each other on a flat surface. Exactness is never expected, but it is possible to achieve very close results. The ultimate goal of calibration is to identify all systematic errors and correct the raw data output so that only random errors remain. Various references are available for more information about Lidar system calibration [1] [2] [3] [4].

¹ National Geodetic Survey, GEOID12A, <http://www.ngs.noaa.gov/GEOID/GEOID12A/>

Table 1 presents the final results for roll and pitch rotation angles. Roll angles represent the discrepancies between overlapping flight lines where pitch correction measures the difference between forward and reverse ($\pm 180^\circ$) scans. The results show that nearly 85% of the errors in the roll were with 3.22 cm or better and that 95% of errors in pitch were 6.87 cm or better. Table 2 lists comparisons between the initial and final measurements registered between laser points on the ground and the absolute surface elevation. These differences occur because of imperfections in the timing of the electronics that measure the laser travel from the transmitter to the ground and back to the receiver. The results show error profiles are within 5-cm vertical accuracy standards set by American Photogrammetry and Remote Sensing Society (ASPRS) [5].

Table 1: Roll and pitch rotation angle discrepancies

Limits (cm)	Average Roll Error (cm)	Percentage (%)	Average Pitch Error (cm)	Percentage (%)
0 <= ERR <2	1	48	1	30
2 <= ERR <5	3	36.5	3.4	37.9
5 <= ERR <10	6.6	11.9	6.8	27.5
10 <= ERR <15	12	2	11.6	3.5
15 <= ERR < Infinite	40	1.6	29	1.1
Summary	3.3	100	4.2	100

Table 2: Comparison of final results with ASPRS 2014 vertical accuracy requirement

	ASPRS 2014 Vertical Accuracy Requirement (cm)	Final DEM accuracy (cm)
NVA 95% Confidence	9.8	8.8
Root Mean Square Error (RMSE _(z))	5	4.5

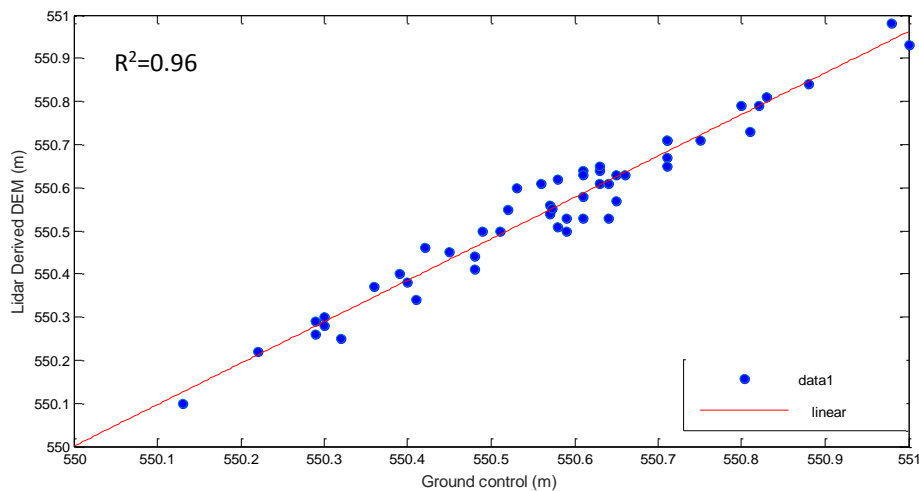


Figure 2: Fit between ground control points and Lidar derived DEM

c) Vegetation Modeling

As stated above in the Introduction section, a primary goal of this research is to improve the predictability of potential desert tortoise habitats using Lidar data, imagery, or a combination of both. The Lidar technology, which is based on light pulses that reflect off the vegetation and return to the aircraft, allows shrub height to be determined, as well as the canopy volume (assuming that the light pulses coincide with the outer portion of the canopy itself). Conversely, the imagery, which was collected in color-infrared (CIR), can distinguish between the tan/brown desert ground surface and the greener vegetation surface, at a high enough resolution (~15 cm pixels) to approximately capture the canopy diameter—but not the height of the shrub canopy. For this reason, both Lidar and imagery together are expected to most accurately portray canopy metrics.

As part of a larger effort by the DCP (and outside of the scope of this project), field crews set up a series of 80 ground-based field plots that could be used for intensive surveys of plant diversity and richness, potential tortoise habitats, etc. These plots are 4 hectares each, and located across the Lidar survey area (see Figure 3) using a handheld Garmin GPS receiver. Figure 4 illustrates the layout of the sample plot, which consists of nested, 1-ha subplots, which are then nested again into 50 x 50 m subplots, into which 30 m long transects, measured from the center point of the plot were chosen. Thus, 4 transects per subplot, or a total of 16 transects per plot were chosen. From discussions with DCP and other scientists working with DCP (Merkler, 2014, personal communication), three of these subplots were selected for field measurements of shrub metrics to be used to validate the Lidar data; these calibration plots are labeled as #7, #22 and #54. Plot 22 is illustrated below in Figure 5, in which the survey area is draped over the color balanced CIR imagery.

Within each of the three subplots, measurements were taken of the dominant vegetation and binned in three general height classes (<50 cm, 50-100 cm, > 100 cm). Vegetation types are identified in Table 3 and specific shrub dimensions are illustrated in Table 4. Figure 6 is an illustration of a creosote bush (*Larrea tridentata*) and a description of dimensions taken of each shrub, in this case to compute canopy volumes of *L. tridentata* [6]. Canopy height is measured from the deposited soil to the approximate overall canopy top. Four different plant species that exist in the three subplots were sampled and identical measurements were taken at each. All field measurements are included in Appendix A. Note that canopy height (H) less than 0.1 m and shrubs with measured canopy size ($\pi(D1/2) \times (D2/2)$) less than 0.25 m² are not included in the study.

Table 3: Shrubs of interest

Latin name	Common name	Code	Identified in Plots
<i>Larrea tridentata</i>	Creosote bush	LATR2	7, 22, 54
<i>Ambrosia dumosa</i>	White bursage	AMDU2	7, 22, 54
<i>Krameria erecta</i>	Purple heather	KRER	22
<i>Yucca schidigera</i>	Mojave yucca	YUSC2	22

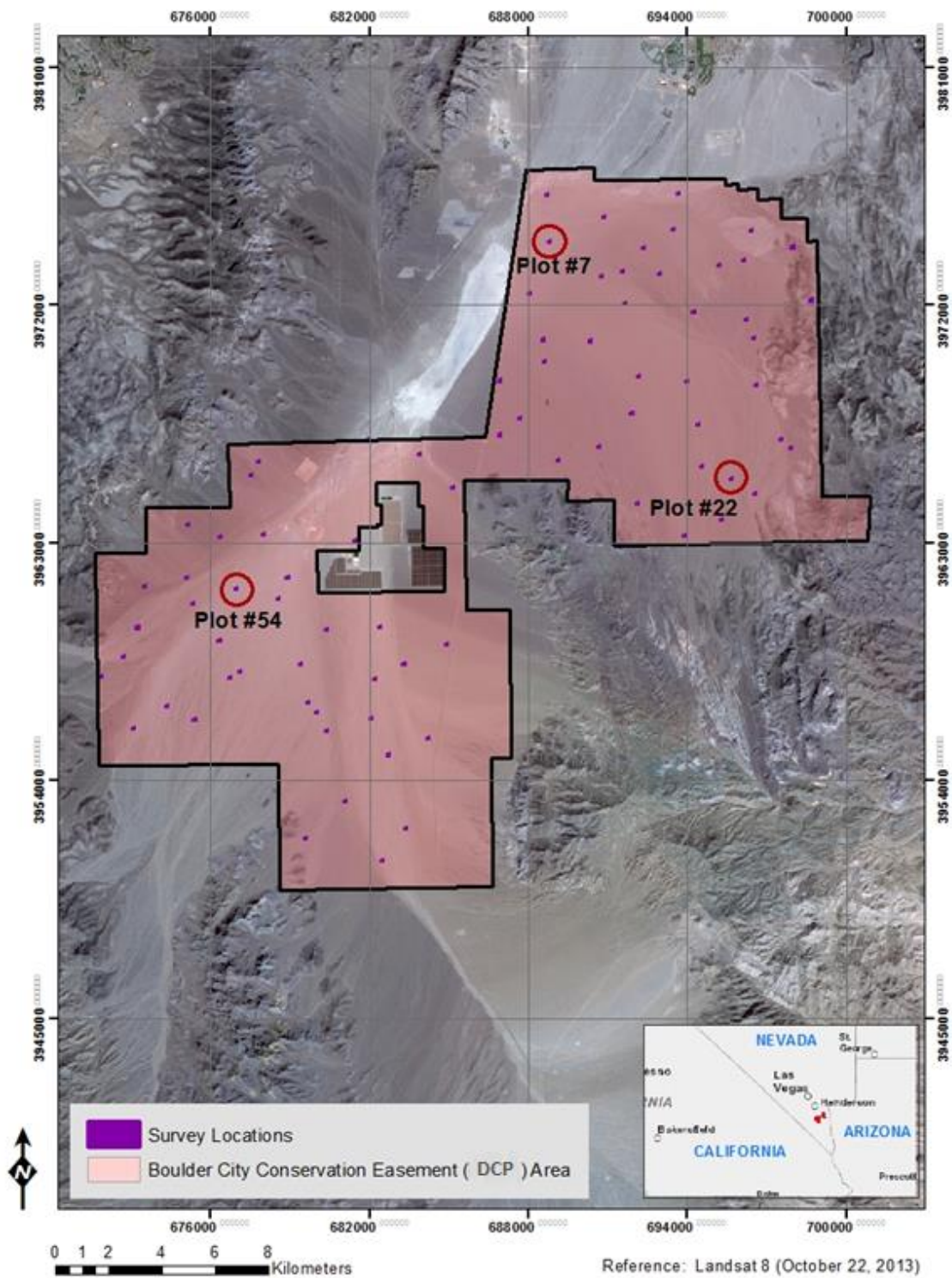


Figure 3: Survey area and the location of designated plots for field vegetation measurements

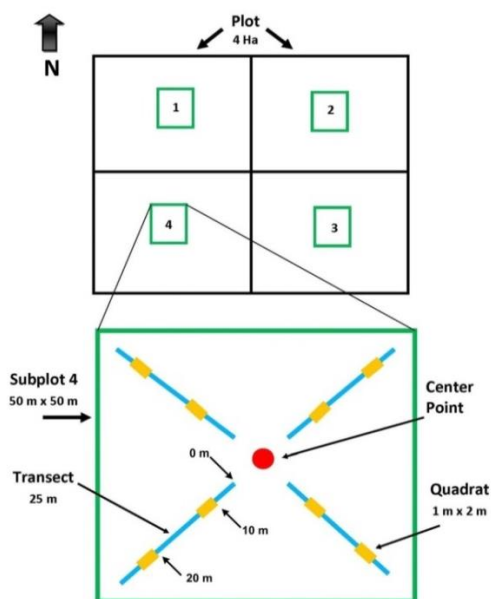


Figure 4: Layout of sampling locations within each subplot

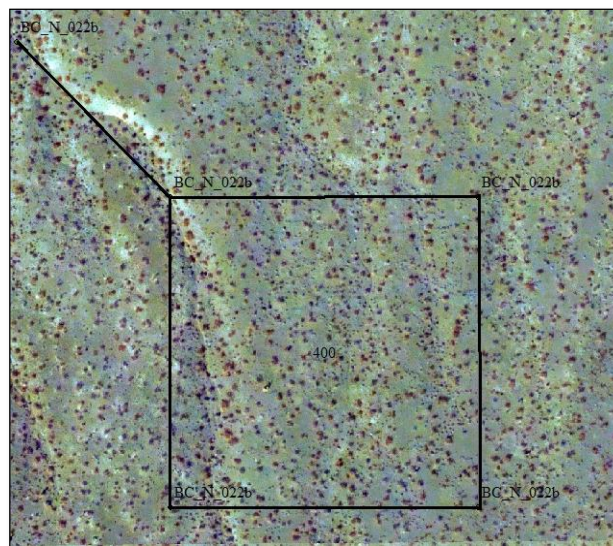


Figure 5: Plot #22 location, draped over color balanced CIR imagery

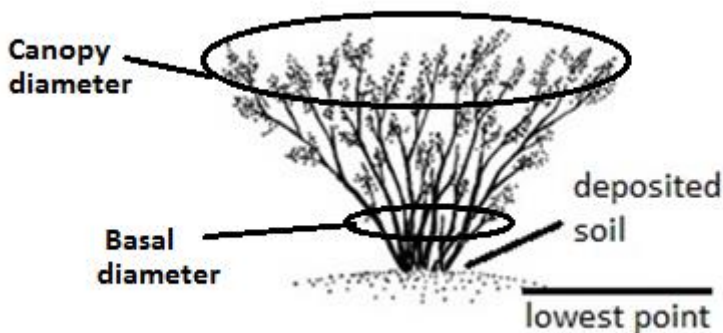


Figure 6: Canopy profile of a creosote bush (after [6]) and measurements taken from each sample bush

Table 4: Measurement parameters for each shrub

Measurement	Parameter	Measurement
Canopy height	H	
Major canopy diameter	D1	Canopy (max)
Minor canopy diameter	D2	Canopy (min)
Major basal diameter	B1	Basal (max)
Minor basal diameter	B2	Basal (min)

d) Geomorphic Features

The study required discovering and measuring of defined geomorphic features; ledges and the overall streamflow in particular. Ledges in geomorphic context are described as surfaces with distinctive vertical surfaces projected from horizontal areas. In this study, ledges were defined as ridges with slopes greater than 70 degrees and with at least 50 cm vertical offset. These features are commonly dug through by desert tortoise to build burrows as shelters, enabling protection from the extreme heat and dryness of the summer, and a place to hibernate in the winter.

Streamflow is the main mechanism by which water discharges to lower elevations or basins. Revealing the streamflow map was considered critical to understand the potential tortoise habitat areas featuring sharp ledges. Map was generated using 1 m bare earth DEM, with distinctive lines to indicate the water flow to lower elevations in the DCP survey location.

e) Computation method

An initial approach was attempted that relied solely on Lidar point cloud data to extract vegetation statistics. However, a limitation to this approach was that our Lidar point density averaged 8 points/m² and our goal was to identify features that were smaller than 1 m². The point cloud data therefore was too sparse to rely on as the sole source of information. To improve reliability of shrub identification, the computations used both Lidar and the imagery data.

First steps taken in the analysis involved preparing both the Lidar data and imagery so they could be properly analyzed. As previously stated, Lidar point cloud data were parsed into 2,000 x 2,000 m tiles and vertically adjusted to NAVD88 using the GEOID12A geoid model. Data in each tile were classified using LAStools as either 'ground' or 'other' and the height of non-ground points above the ground surface were determined. These points were then rasterized at 0.5 m resolution and recorded as Band Interleaved by Line (BIL) format. The imagery were parsed into same size tiles to match the Lidar data and were also saved in BIL format.

The next step required identification of individual plants in the imagery and Lidar data using software written in the house. The software works as follows:

- A pseudo Normalized Difference Vegetation Index (NDVI) calculation $(\text{Green} - \text{Red}) / (\text{Green} + \text{Red})$ is run on the imagery to identify vegetation in the RGB data; positive values ($> 0, \leq 1$) indicate vegetation (Figure 7).
- We employ a cluster algorithm to group contiguous positive NDVI returns into clusters representing individual plants. After experimenting with different methods and parameters, we settled on the following steps:

- A first pass identifies all contiguous cell clusters > ~0.25 m² with NDVI values > 0.2 (Figure 8). Each cluster's center coordinate and area are calculated and stored in RAM.
- A second pass identifies all contiguous cell clusters > ~0.25 m² with NDVI values > 0.0 and < 0.2 (Figure 9); again the center coordinate and area are stored.
- Finally, all second pass clusters are re-evaluated, and those clusters whose center coordinate lay within 1.3 m of a first pass point are considered redundant and deleted (Figure 10).
- Each cluster's footprint is cross-referenced to the Lidar data and the greatest coincident height value is stored. For each tile, these findings were written out as text files in the format presented with Table 5. After all the tiles were processed, individual text files were merged into a single file that represented results for the entire study area. Vegetation density maps were generated with Global Mapper v15 using the "Create Density Grid" utility (Figure 12).

Table 5: Sample result for each computed vegetation

#	Latitude (UTM z11N)	Longitude (UTM z11N)	Height (m)	Area (m ²)
1	670181.79	3957999.52	0.81	0.70
2	670150.77	3957999.91	0.42	0.56
3	670075.85	3957999.75	0.92	0.60
4	670877.53	3957999.78	0.02	0.33
5	670431.34	3957999.59	0.51	0.28

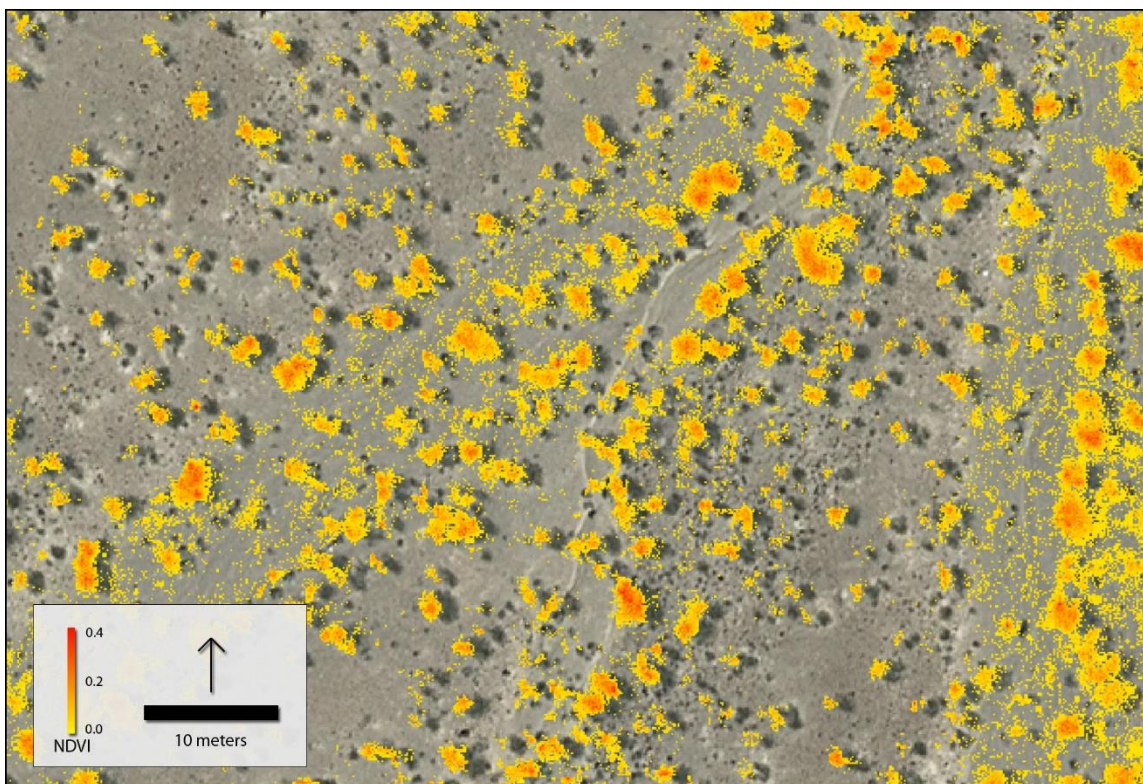


Figure 7: Colored areas represent clusters where pseudo NDVI formula returned positive values to indicate vegetation

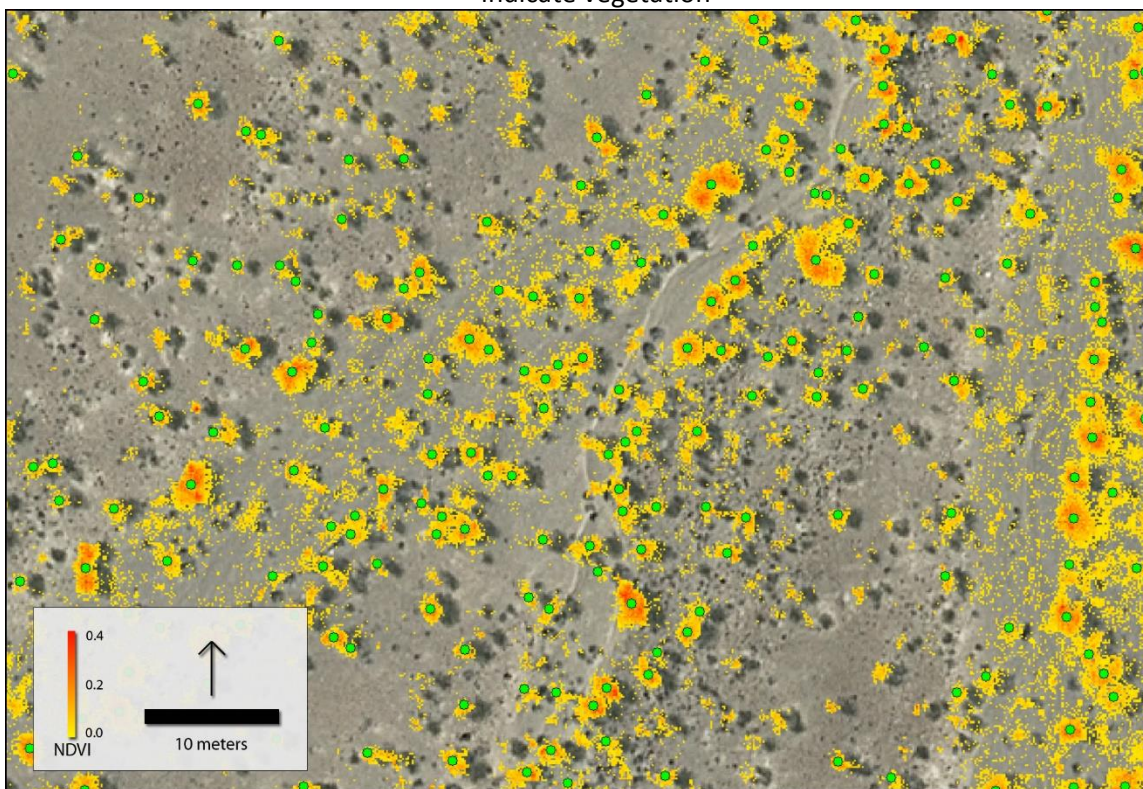


Figure 8: NDVI returns cell clusters $> \sim 0.25\text{m}^2$, NDVI values > 0.2

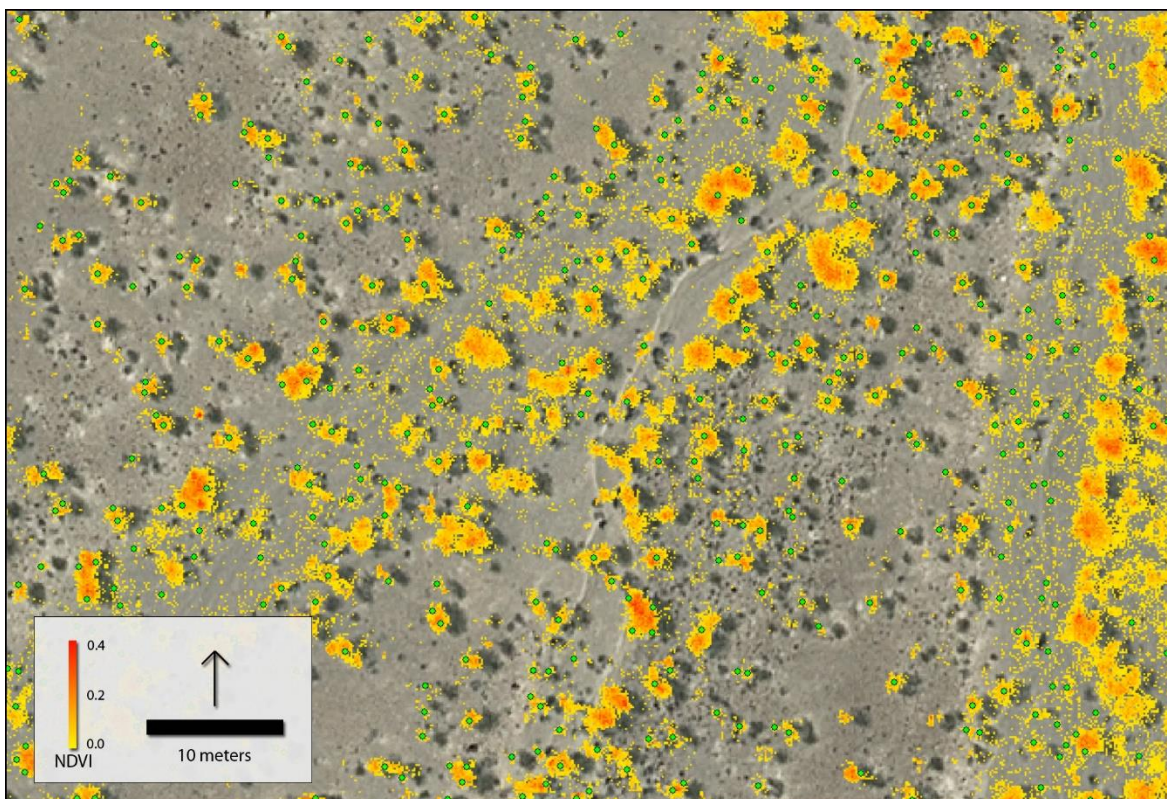


Figure 9: NDVI returns cell clusters $> \sim 0.25\text{m}^2$, NDVI values > 0 and < 0.2

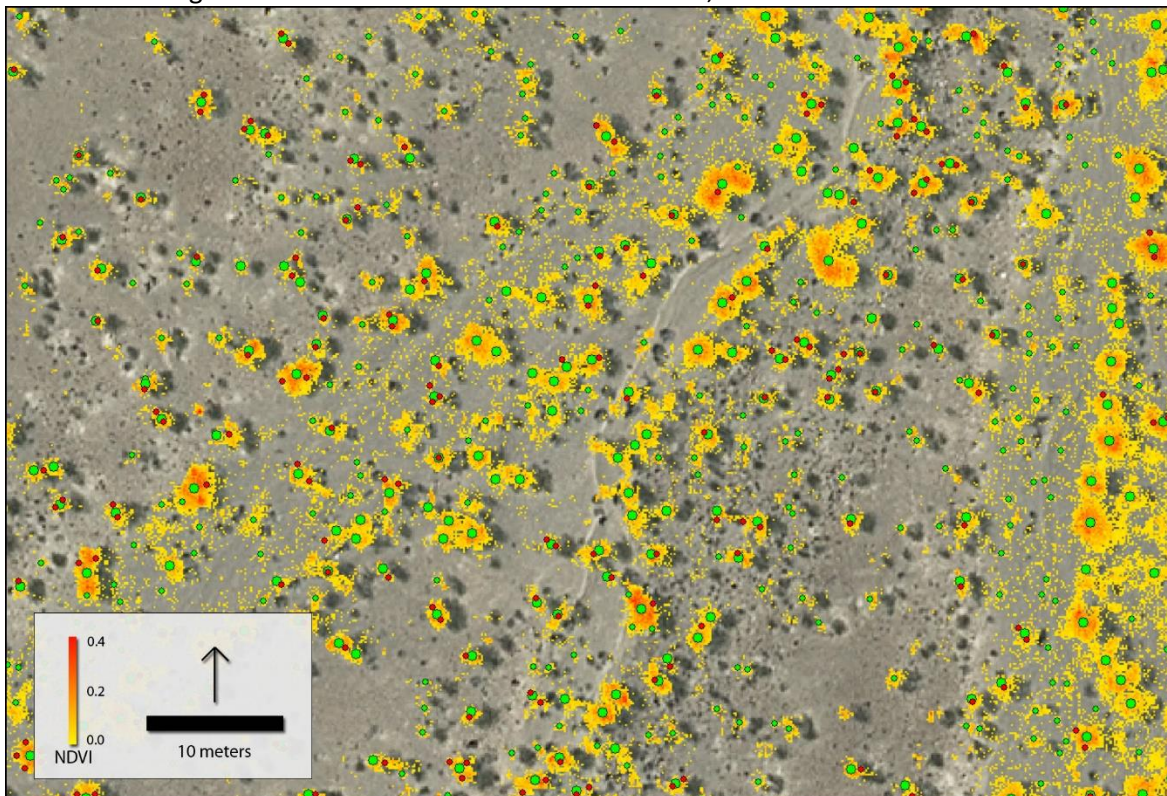


Figure 10: Removed clusters represented with red dots

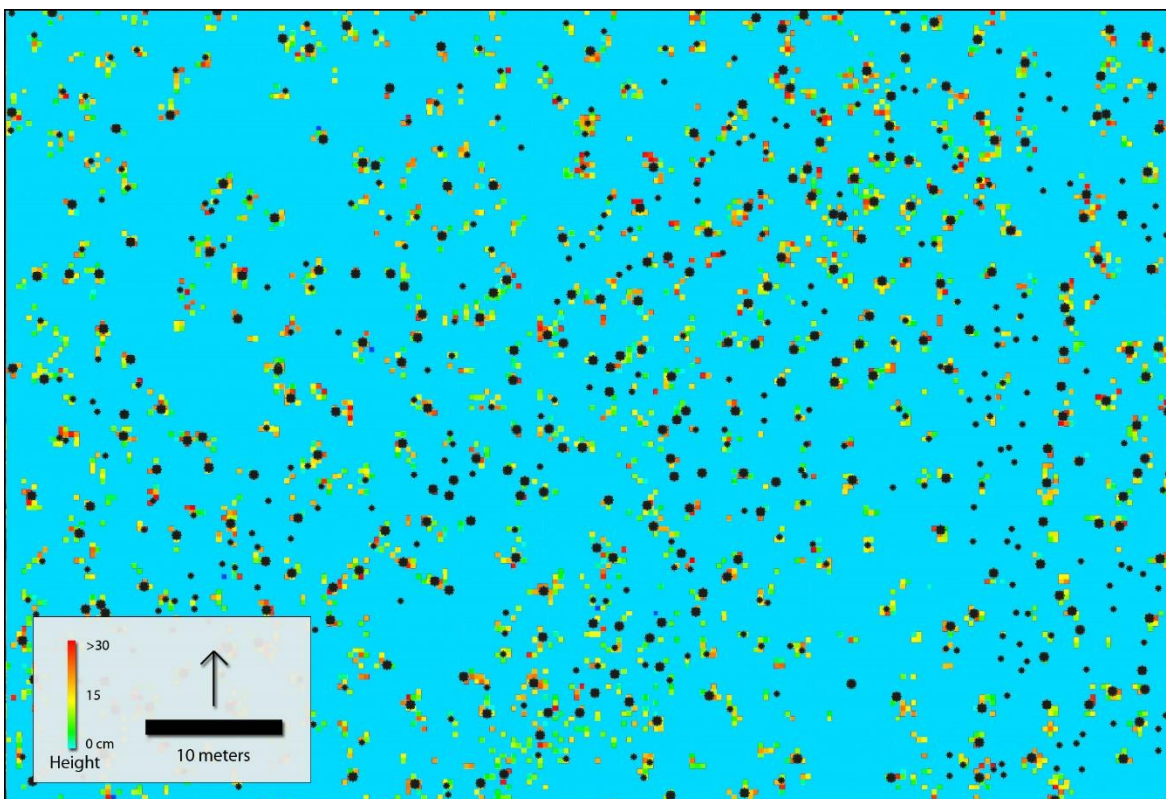


Figure 11: Black dots represent vegetation found with NDVI and their cross reference with Lidar point cloud data

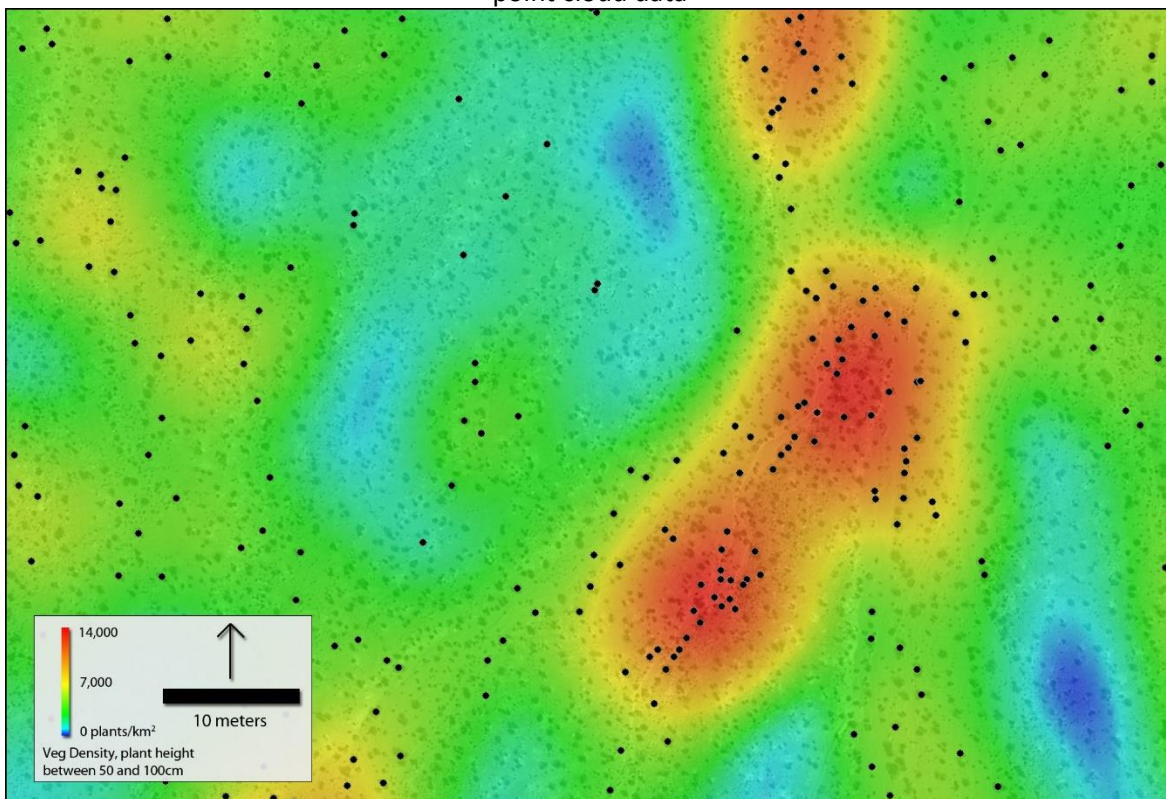


Figure 12: Vegetation density as defined by 10 m radius from each

3) Results and Discussion

a) Digital Elevation Model

A Digital Elevation Model (DEM) is created by 1,000 x 1,000 m grids by sampling 1 m point density. Original 2,000 x 2,000 m grids were deemed as too large and heavy for ordinary computers. Tiles were created with edges extended 20 m as a buffer for building seamless tiles. Figure 13 presents the entire DEM for DCP area, with an emphasis on an area with apparent elevation changes.

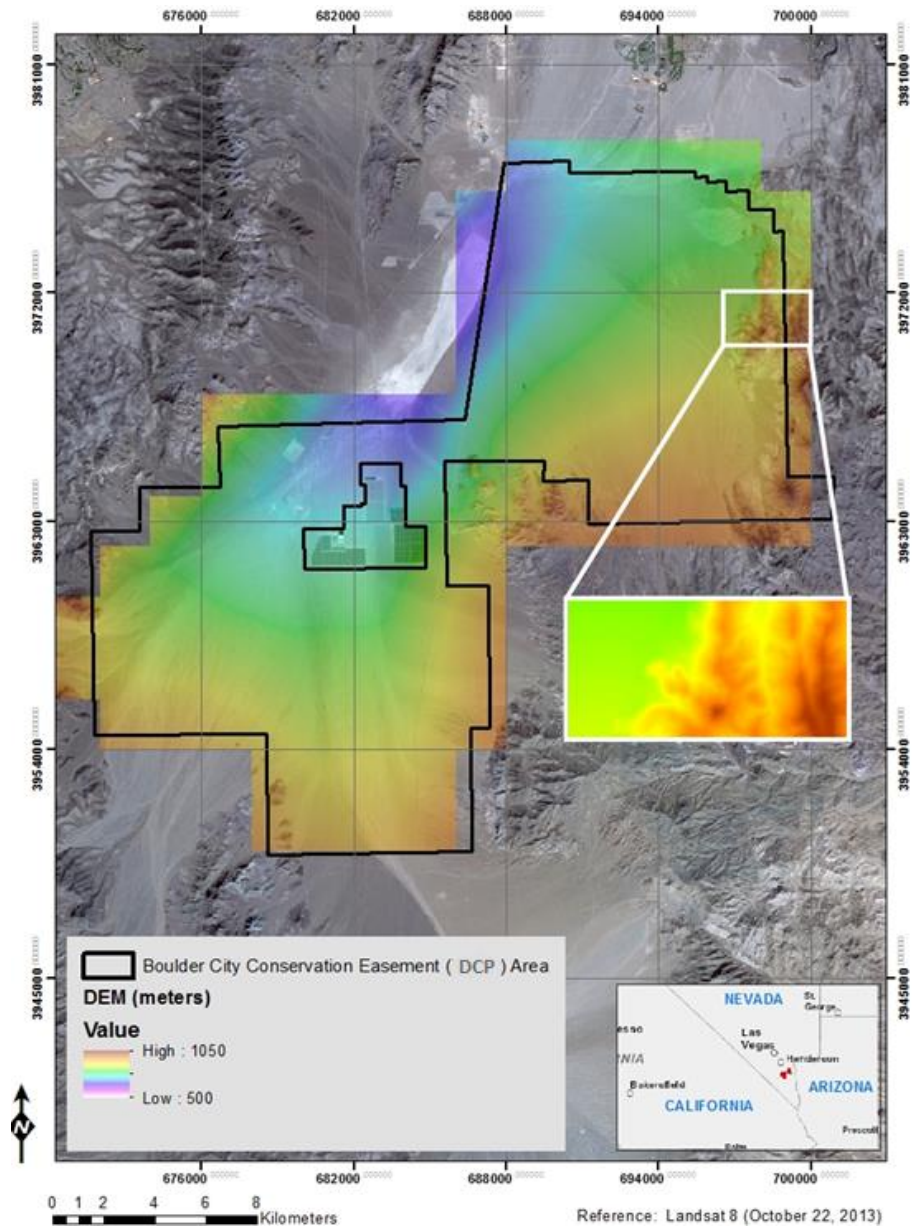


Figure 13: DEM for entire DCP survey area and sample DEM from NE corner

b) Field Measurements

Table 6 represents the sample values measured in the field as described previously with conventional methods. Figure 14 presents the average values of each vegetation type at their respective plot location. The results show that species diversity was limited at Plots 7 and 54, where KRER and YUSC2 were not found or sampled. Results also show highest average canopy heights at Plot 22 for each vegetation type, which could indicate a more stable growth environment allowing shrubs to mature and grow to their maximum height, given meteorological and soil conditions.

Table 6: Dimensions of vegetation measured in the field

Vegetation	Basal (cm)		Canopy (cm)		# samples
	Avg. Min	Avg. Max	Avg. Min	Avg. Max	
AMDU2	16.9	25.1	48.8	65.6	18
LATR2	35.7	57.3	108.2	147.7	18
KRER	14.8	27.1	45.3	65.6	6
YUSC2	42.7	72.0	80.9	109.2	6

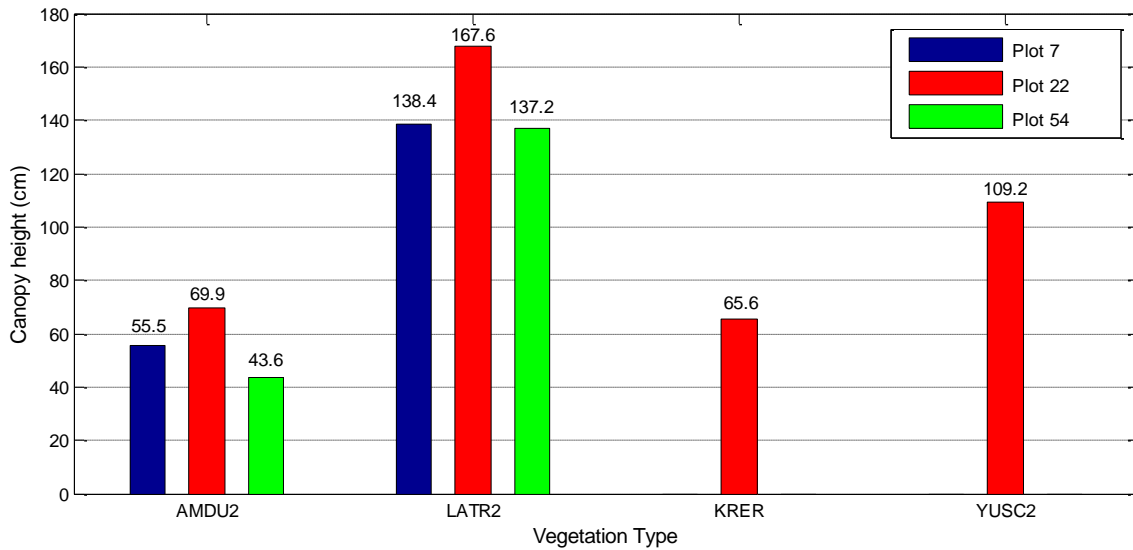


Figure 14: Average maximum canopy height (cm) for each vegetation type in each plot

c) Computational Findings

In summary, 82% of all vegetation identified in the three plots was shorter than 0.5 m and with less than 1 m² canopy area. The remaining 18% of the shrubs were taller than 0.5 m and with a canopy area larger than 1 m². Tallest average canopy height was recorded in Plot 54 (average = 0.35 m). Average canopy area was largest in Plot 22 (mean value = 0.76 m²), and smallest in Plot 54 (mean value = 0.41 m²). A total of 116 shrubs were identified with canopy areas larger than 1 m².

Figure 15 collates the results of plant height identification for all three plots. The graph was created by summing all the plants identified in each plot, using Lidar returns as the data source, and sorting them by height. The results show some interesting differences between plots. First, substantial differences exist in the number of shrubs, with the largest number of shrubs (435) identified with Lidar in Plot 22, found mid-way up the fan surface versus the least number of shrubs (125) identified in plot 54, located near the valley floor. The number of shrubs found at Plot 7 (320) is between the two. Second, we noted the number of shrubs identified per 100 m² is much lower than seen elsewhere in the Mojave Desert. For example, we identified 1.09, 0.80 and 0.31 shrubs/100 m² at Plots 22, 7, and 54, respectively; whereas, Hamerlynck [7] reported values of >2.0 plants/100 m² just for *L. tridentada* on nearly all alluvial fan surfaces studied at the Mojave National Preserve, southwest of Eldorado Valley. The low numbers of shrubs are important because this limits the potential habitats available for the tortoise. Finally, we note the relatively small number of shrubs with heights above 50 cm, and only three shrubs measured at >1 m height across all three plots. We noted that shrubs with heights >50 cm, when represented as a percentage of total number of shrubs, also differed by plot. For example, percentages were 1.25%, 3.2%, and 16% for Pots 22, 54, and 7, respectively. Thus, though the absolute number of shrubs near the playa is lowest of the three plots, Plot 7 does have the largest number and highest percentage of larger shrubs.

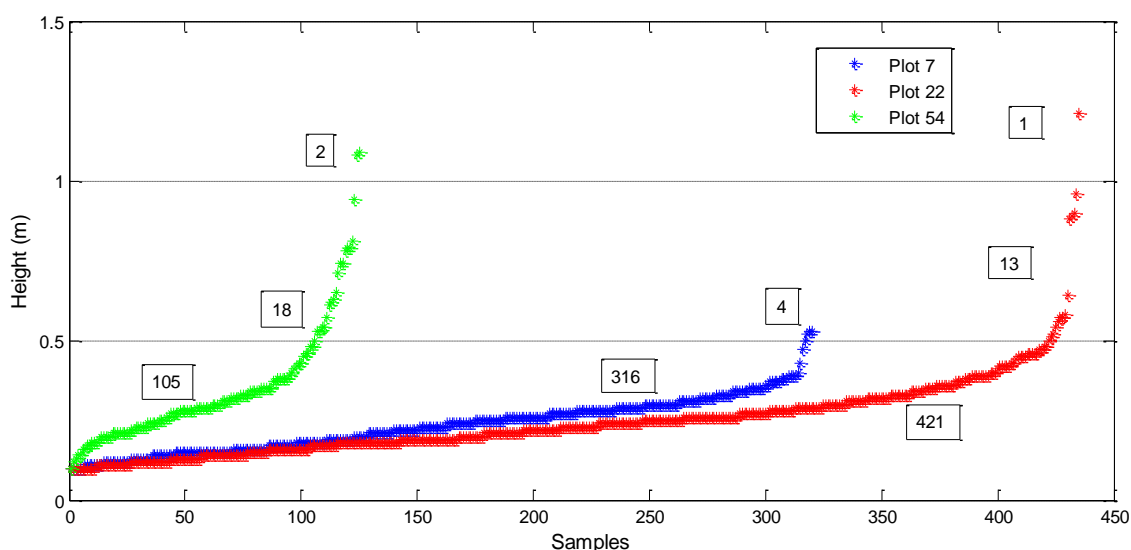


Figure 15: Canopy height comparisons; values in boxes represent the number of samples in each 0.5 m bin

Figure 16 presents results in which canopy area, shown in units of m^2 , is shown for each plot. Note that canopy area was determined using imagery analysis with a pixel resolution of 15 cm (i.e., Lidar data was not used). As above, the results show substantial differences in the characteristics of canopy area at these studied plots. Plot 22 has 20 shrubs with areas $>2.0 m^2$, which could indicate that these locations were subjected to collocation of shrubs and/or concentrations of nutrients that would lead to “islands of fertility” a term coined by Schlesinger [8] and later discussed by others ([9] [10] [11]). The other plots did not exhibit the prevalence of shrub islands to any great extent, possibly because the soil profiles were less developed. We also noted the interesting shapes of the traces shown on Figure 16, and that they can accurately be described by a third-order polynomial. For example, for Plot 22, a polynomial can be fitted to the data that yields an $R^2=0.931$ (not shown on Figure 16), though the physical significance of the curve fitting and coefficients is not well understood. Finally, if we consider the normalized area occupied by shrubs on each of the three plots (as expressed by the vertically downward projection using imagery analysis), we found that the values were quite similar for Plots 7 and 22 (152.5 and $154.3 m^2/ha$), both of which were found on the steeper portions of the fan, and about three times higher than measured for the Plot 54 ($51.3 m^2/ha$) found on the gentler sloped portion of the fan, nearer the playa. From the standpoint of habitats, the larger number of potentially larger shrub islands and overall coverage could provide better habitats for tortoises.

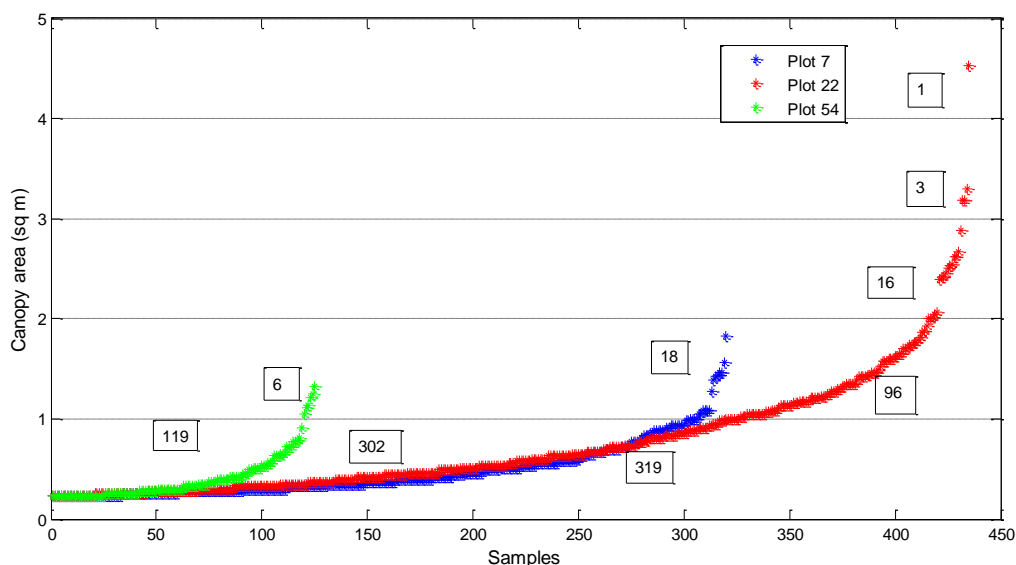


Figure 16: Canopy area comparison; box values indicate total samples calculated in each $1 m^2$ bin

Figure 17 represents canopy height (H) versus canopy area [calculated as $area = \pi (D1/2) \times (D2/2)$] for all three plots studied, and as determined by Lidar for canopy height and imagery analysis for canopy area. The results show considerable scatter of the data, which perhaps is not surprising given the comparison of results from two remote sensing technologies. Using linear regression to assess canopy area as a function of canopy height, we found correlation coefficients (r^2) increasing from 0.132 to 0.139 to 0.206 for Plots 22, 7 and 54, respectively. We found also that standard errors of the estimate for canopy area varied, respectively, from 0.54 to 0.25 to $0.21 m^2$. As illustrated in Figure 18, the density of small shrubs is higher in Plots 7 and 22. Tables 7 and 8 summarize findings of each plot.

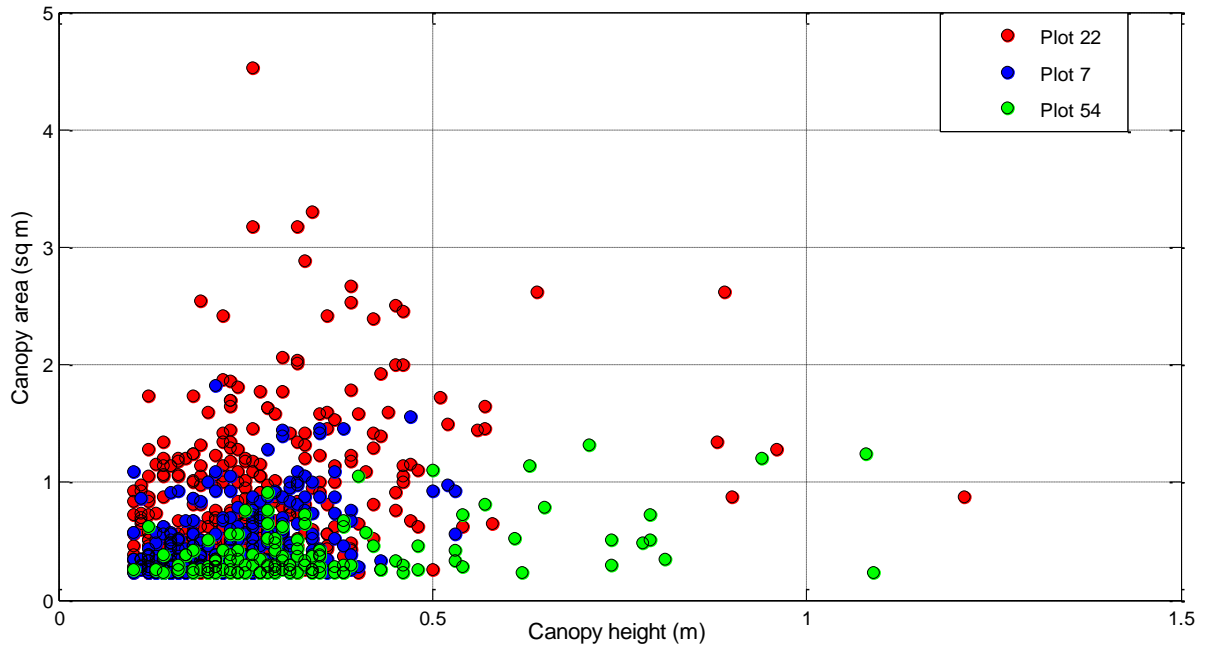


Figure 17: Canopy area versus canopy height in all plots

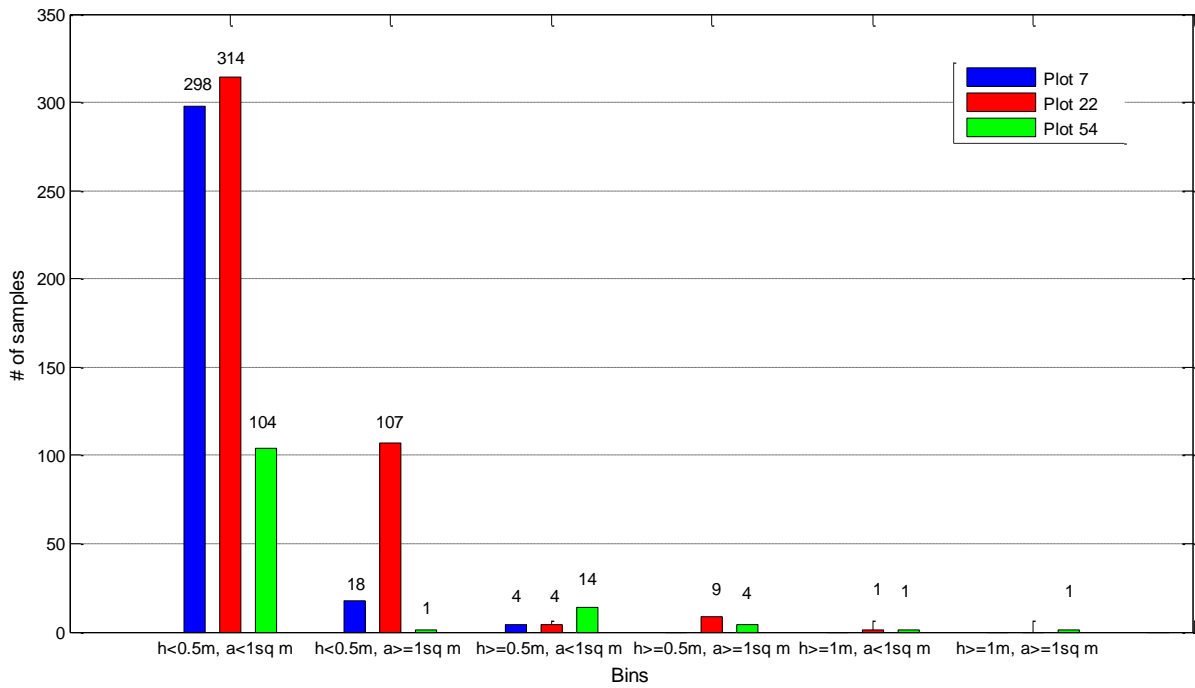


Figure 18: Number of samples in each bin for canopy height (m) versus canopy size (m²)

Table 7: Canopy height comparison for all plots

	# samples	Min (m)	Max (m)	Mean (m)	Standard Deviation (m)	< 0.5 (m)	0.5-1.0 (m)	≥ 1.0 (m)
Plot 7	320	0.1	0.53	0.23	0.08	316	4	N/A
Plot 22	435	0.1	1.21	0.25	0.12	421	13	1
Plot 54	125	0.1	1.09	0.35	0.18	105	18	2

Table 8: Canopy area comparison for all plots

	# samples	Min (m ²)	Max (m ²)	Mean (m ²)	Standard Deviation (m ²)	< 1.0 (m ²)	≥ 1.0 (m ²)
Plot 7	320	0.23	1.83	0.47	0.27	302	18
Plot 22	435	0.23	4.53	0.76	0.58	319	116
Plot 54	125	0.23	1.32	0.41	0.23	119	6

d) Other Features of Interest; Ledges and Stream Networks

In this study, ledges were defined as features with slopes greater than 70 degrees and with at least 50 cm of vertical offset, using hillshade bare earth DEM as input. We also assessed the impact of DEM resolution by analyzing for ledges using a 1 m bare earth DEM resolution, and then again at a 4-fold higher resolution of 0.25 m. Calculations using the 1 m bare earth DEM yielded no ledges across the entire study area. This result stems from the fact that using the 70 degrees slope criteria would have led to a required vertical offset of 46.7 cm for each 1 m lateral offset. On these gently sloping alluvial fans, and with these criteria, no vertical ledges were identified (Fig. 19). Increasing the resolution with tighter lateral offset of 0.25 m led to significantly more areas identified as ledges (Fig. 20). The cross section shown in Figure 21 also reveals the vertical landscape and the significant difference at the sample location depending solely on the resolution of the DEM. However, for study purposes, we calculated the ridges that have greater slope than 50 degrees. Though computationally more intensive, the results are more useful.

Figure 22 presents an example of streamflow map generated using bare earth 1 m DEM. For this purpose, it is sufficient to use 1 m bare earth DEM since flow channels in the area were highly visible due to geomorphologic features in the desert. Data is produced and provided as an ESRI shapefile and it can be used as a supplemental source for finding the locations of the ledges that are mostly clustered by the water flow channels.

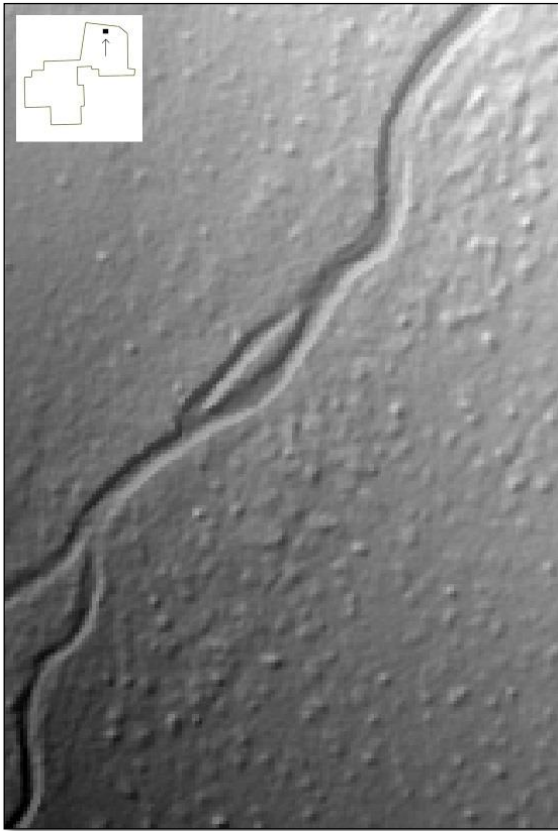


Figure 19: 1 m DEM did not reveal any ledges

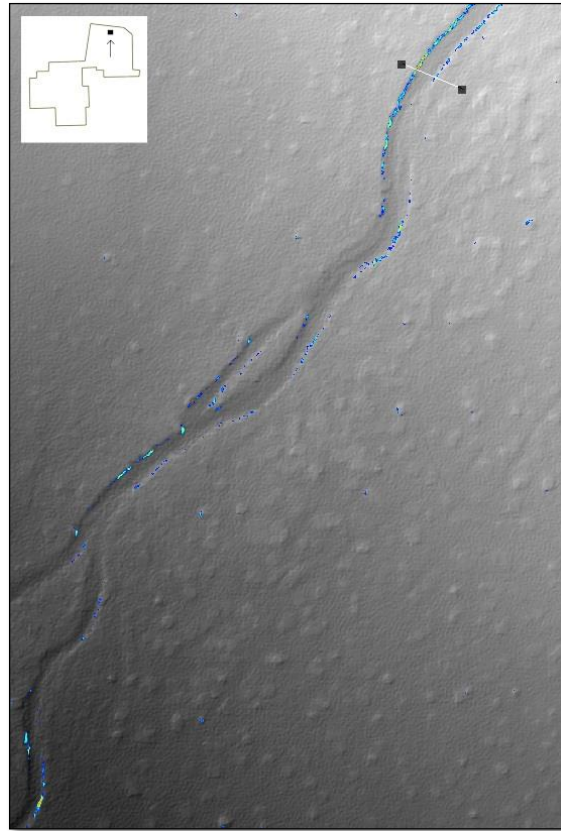


Figure 20: Cross section over distinctive ledges were generated with 0.25 m DEM

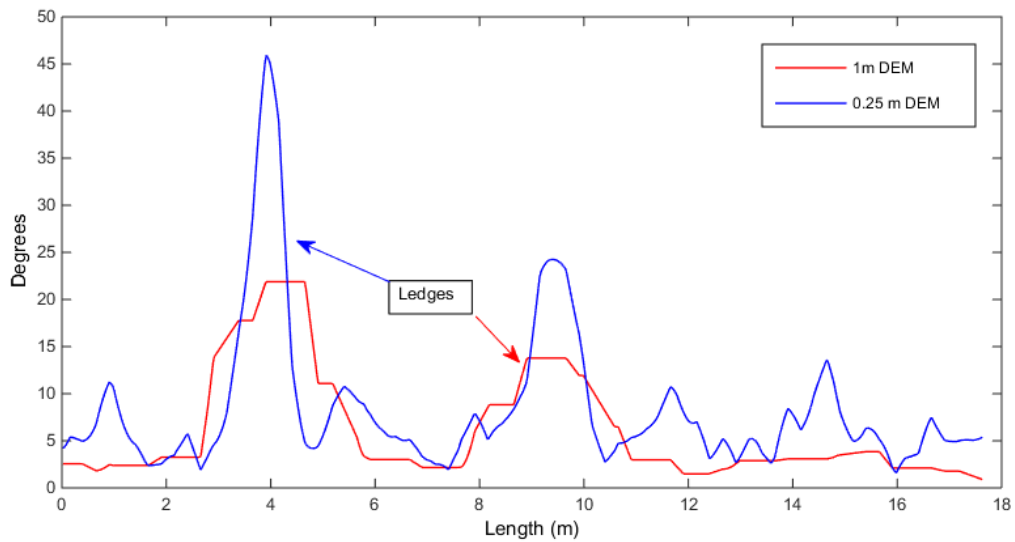


Figure 21: Ledges were generated from 1 m and 0.25 m DEM reveal significant vertical profile differences (see cross section as shown on Fig. 20)

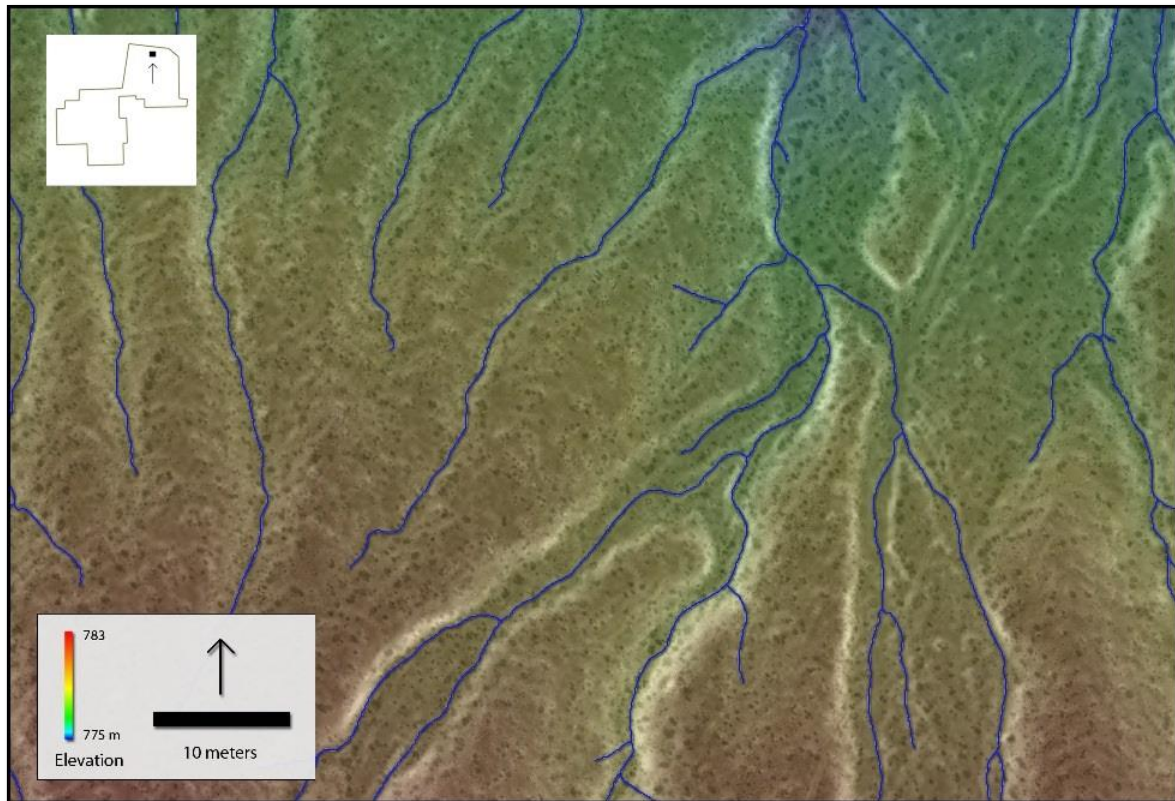


Figure 22: Stream networks generated from bare earth DEM

4) Conclusion

The goal of this study was to analyze previously collected Lidar data and imagery, to develop a fine-scale model that would help to predict potential habitat locations of the endangered desert tortoise in the DCP. Airborne Lidar data and aerial imagery complemented each other to predict the results and to generate the results as presented in this paper. The advanced analysis completed herein estimated vegetative height, canopy area and species richness of four different plant species in three selected plots. Shaded areas will be determined and submitted with the final report after discussions and field verification.

Our findings reveal different vegetation characteristics and potential habitat environments across the three plots, which originally were chosen based on their different locations on the alluvial fan surface that dominates northern Eldorado Valley. For example, the results indicate higher species richness, with all four growth forms present only on Plot 22, and with only *L. tridentata* and *A. dumosa* observed on Plots 7 and 54. Without the benefit of significant field observations, we suggest that Plot 22 is found on a fan piedmont or fan remnants, and using the USDA SSURGO database, this would indicate the presence of an Arizo soil (sandy-skeletal, mixed, thermic Typic Torriorthents) with high sand percent, low runoff potential and enough horization to support a significant B horizon. Plots 7 and 54 are found on either alluvial flats or skirts, and this would suggest a younger soil without significant horization (such as the Hypoint series). Differences of vegetation on these surfaces could be explained by the different soil materials or the stability of the soil profile from erosion or deposition, thereby providing enough time for a more complex and rich vegetation assemblage to develop. The results show clear differences in canopy structure in all three plots, with a larger number of shrubs overall, and a larger area of shrubs with area > 2 m², possibly indicating the development of more robust fertility islands and recruitment of different growth forms that co-associate with *L. tridentata*. The younger soils likely found at Plots 7 and 54, may not be stable enough for larger shrub islands to develop. These results suggest the potential to map suitable vegetation structure on the basis of geomorphic terrain and/or soil profile properties, and hence the preferential identification of suitable habitats for the desert tortoise.

These results need additional field verification, particularly the measurement of canopy height. The Lidar measurement method can provide highly accurate DEMs, and identify the location of shrubs, but use of this technology for accurately measuring canopy height may depend on the random likelihood that the light pulse exactly hits the uppermost leaf or branch. Without extremely high resolution measurements, that were not possible on this survey, we cannot state with high confidence that the exact heights of individual shrubs are correct. Field measurements of specific shrubs, and then checking the Lidar-derived canopy height, would provide the means to improve estimates of all shrubs in the survey area, and potentially identification of tortoise habitats.

Acknowledgements

Authors would like to thank everybody involved in the study. The study was sponsored by the Clark County Desert Conservation program, Las Vegas, NV, under contract number CBE 603383-14. Flight services were provided by Aspen Helicopters of Oxnard, California. Bureau of Economic Geology research staff Aaron Averett operated the airborne Lidar system and John Andrews provided ground GPS control support in Nevada. Tiffany Caudle, Rebecca Brown and John Hupp provided overall assistance with data processing and QC.

Appendix A – Field vegetation measurement

Plot#	Point ID	Northing	Easting	USDA Code	Basal (cm)		Canopy (cm)		Canopy Height (cm)	
					Min	Max	Min	Max	Lowest point	Deposited soil
54	3	676869	3961346	AMDU2	10.2	20.3	53.3	71.1	38.1	33.0
54	4	676871	3961330	AMDU2	30.5	35.6	76.2	86.4	50.8	40.6
54	5	676873	3961327	AMDU2	10.2	12.7	33.0	50.8	38.1	33.0
54	6	676872	3961325	AMDU2	10.2	12.7	45.7	53.3	33.0	33.0
54	7	676879	3961323	LATR2	25.4	66.0	99.1	139.7	88.9	83.8
54	8	676877	3961312	LATR2	15.2	27.9	86.4	116.8	73.7	58.4
54	9	676902	3961319	LATR2	27.9	53.3	109.2	167.6	111.8	109.2
54	10	676915	3961320	LATR2	20.3	22.9	78.7	86.4	63.5	61.0
54	11	676885	3961374	LATR2	15.2	76.2	167.6	233.7	94.0	86.4
54	12	676893	3961374	LATR2	10.2	15.2	48.3	78.7	86.4	76.2
54	13	676917	3961345	AMDU2	22.9	35.6	45.7	68.6	43.2	33.0
54	14	676929	3961324	AMDU2	25.4	38.1	68.6	99.1	58.4	40.6
7	15	688708	3974433	LATR2	38.1	55.9	94.0	144.8	134.6	78.7
7	16	688717	3974420	LATR2	40.6	61.0	88.9	144.8	83.8	83.8
7	17	688720	3974403	LATR2	45.7	73.7	119.4	162.6	86.4	71.1
7	18	688732	3974392	LATR2	48.3	86.4	96.5	99.1	162.6	172.7
7	19	688714	3974383	LATR2	38.1	45.7	83.8	116.8	91.4	83.8
7	20	688735	3974365	LATR2	50.8	78.7	96.5	162.6	78.7	71.1
7	21	688715	3974381	AMDU2	10.2	25.4	33.0	48.3	25.4	20.3
7	22	688701	3974380	AMDU2	10.2	10.2	35.6	43.2	30.5	30.5
7	23	688713	3974399	AMDU2	22.9	27.9	35.6	40.6	25.4	30.5
7	24	688685	3974400	AMDU2	30.5	35.6	45.7	68.6	40.6	27.9
7	25	688729	3974424	AMDU2	22.9	33.0	48.3	66.0	38.1	25.4
7	26	688709	3974429	AMDU2	20.3	40.6	35.6	66.0	38.1	30.5
22	27	695700	3965494	LATR2	30.5	58.4	83.8	127.0	94.0	81.3
22	28	695697	3965488	LATR2	17.8	45.7	160.0	180.3	109.2	99.1
22	29	695682	3965477	LATR2	22.9	45.7	119.4	180.3	91.4	81.3
22	30	695664	3965466	LATR2	106.7	104.1	177.8	223.5	111.8	88.9
22	31	695671	3965463	LATR2	45.7	45.7	132.1	180.3	180.3	139.7
22	32	695651	3965463	LATR2	43.2	68.6	106.7	114.3	63.5	61.0
22	33	695656	3965460	AMDU2	10.2	12.7	63.5	68.6	35.6	33.0
22	34	695670	3965461	AMDU2	17.8	35.6	58.4	76.2	38.1	33.0
22	35	695666	3965451	AMDU2	10.2	12.7	76.2	81.3	38.1	33.0
22	36	695691	3965437	AMDU2	17.8	27.9	33.0	66.0	40.6	35.6
22	37	695695	3965436	AMDU2	7.6	10.2	35.6	43.2	27.9	27.9
22	38	695704	3965442	AMDU2	15.2	25.4	55.9	83.8	33.0	33.0
22	39	695700	3965441	KRER	12.7	20.3	45.7	55.9	22.9	22.9
22	40	695700	3965431	KRER	15.2	25.4	30.5	50.8	22.9	20.3
22	41	695700	3965422	KRER	15.2	38.1	48.3	76.2	15.2	12.7
22	42	695699	3965416	KRER	7.6	33.0	35.6	73.7	22.9	20.3
22	43	695703	3965408	KRER	12.7	20.3	55.9	66.0	35.6	33.0
22	44	695707	3965398	KRER	25.4	25.4	55.9	71.1	22.9	20.3
22	45	695688	3965376	YUSC2	53.3	88.9	88.9	129.5	121.9	
22	46	695702	3965376	YUSC2	40.6	78.7	81.3	121.9	109.2	
22	47	695724	3965375	YUSC2	22.9	35.6	71.1	91.4	86.4	
22	48	695724	3965382	YUSC2	30.5	30.5	81.3	81.3	101.6	
22	49	695738	3965389	YUSC2	58.4	119.4	91.4	144.8	111.8	
22	50	695730	3965406	YUSC2	50.8	78.7	71.1	86.4	88.9	

Appendix B – C++ and AWK Code

C++ code: This algorithm is written to find clusters of high NDVI values in the imagery data “ras_ndvic” and co-locate the same areas in the lidar data “ras_hi” to extract the height information. This algorithm outputs a text file of all the plants found, including those that will later be deleted with the AWK algorithm.

```
void proc_find_reg_over_getVal( rast *ras_ndvic, rast *ras_hi, uint8 minVal, uint16 minRegSize, f64 xMinCl, f64 yMinCl, f64 xMaxCl, f64 yMaxCl, char *oVec )
{
    uint16 fileEdgeBuff = 2;

    uint16     *spiCoord; // spider coordinate pairs in column units (a,b)
    uint8      *spiCoord_AT; // spider coordinate Already There

    uint8      TARGET;

    float      nData = ras_ndvic->get_nData();
    uint16     nCols = ras_ndvic->get_nCols();
    uint16     nRows = ras_ndvic->get_nRows();
    f64        xMin = ras_ndvic->get_xMin();
    f64        yMax = ras_ndvic->get_yMax();
    f32        xDim = ras_ndvic->get_xDim();
    f32        yDim = ras_ndvic->get_yDim();

    f64        xCoord, yCoord;

    FILE *fp;
    fp = fopen(oVec,"w");
    if(fp == 0)
    {
        fprintf(stderr, "ERROR: cannot open for writing file %s\n", oVec);
        exit(1);
    }
    fprintf(fp, "id,x,y,height_m,area_m2,class\n");

    if(xMinCl == -9999)
    {
        xMinCl = -99999999;
        xMaxCl = 99999999;
        yMinCl = -99999999;
        yMaxCl = 99999999;
    }

    uint32 spiCoordArraySIZE = nCols*nRows*2;
    uint32 spiderNUM = 0;

    TARGET = minVal;

    uint16 prevTarX;
    uint16 prevTarY;
    uint16 x;
    uint16 y;

    jstack <pt_ui16> holds(spiCoordArraySIZE/2);
    spiCoord = new uint16[spiCoordArraySIZE];
    spiCoord_AT = new uint8[nCols*nRows];

    uint32 tarSpiCOUNT; // target COUNT per spider
    uint16 tarWinCOUNT; // target COUNT per 3x3 window
    uint32 tarTotCOUNT; // target COUNT total
    uint32 tarNonCOUNT; // non-target COUNT
    pt_ui16 pt_temp;
```

```
uint32 gtRegCOUNT = 1; // greater than MinReg COUNT

// -- Initialize spiCoord;
for( uint32 a = 0; a<spiCoordArraySIZE; a++)
    spiCoord[a] = 0;

// -- Initialize spiCoord_AT; note: buffer'ed area TRUE, else FALSE
for( uint16 b = 0; b<nRows; b++)
{
    for( uint16 a = 0; a<nCols; a++)
    {
        if( (a<filEdgeBuff) || (a>(nCols-filEdgeBuff)) || (b<filEdgeBuff) || (b>(nRows-filEdgeBuff)) )
            spiCoord_AT[(b*nCols)+a] = 1;
        else
            spiCoord_AT[(b*nCols)+a] = 0;
    }
}

tarTotCOUNT = 0;
tarNonCOUNT = 0;

for( uint16 t = 0; t < 2; t++)
{

    if(t==0)
        TARGET = 25; // 25 in uint8 array = ~.2 in floating point NDVI
    else
        TARGET = 2;

    for(uint16 b = (0+filEdgeBuff); b < (nRows-filEdgeBuff); b++)
    {
        for(uint16 a = (0+filEdgeBuff); a < (nCols-filEdgeBuff); a++)
        {

            tarSpiCOUNT = 0;

            if( (ras_ndvic->get_rasDat_c(a,b,0) >= TARGET) && (spiCoord_AT[(b*nCols)+a] != 1) )
            {

                spiderNUM++;

                while ( (tarSpiCOUNT == 0) || (tarWinCOUNT != 0) || (holds.get_p() != 0) )
                {

                    if(tarSpiCOUNT == 0)
                    {
                        x = a;
                        y = b;
                    }
                    else if( tarWinCOUNT != 0 )
                    {
                        x = prevTarX;
                        y = prevTarY;
                    }
                    else
                    {
                        pt_temp = holds.pop();
                        x = pt_temp.x;
                        y = pt_temp.y;
                    }
                }

                tarWinCOUNT = 0;

                for(int16 n=-1; n<=1; n++)
```

```
{
for(int16 m=-1; m<=1; m++)
{
if(ras_ndvic->get_rasDat_c((x+m),(y+n), 0) >= TARGET)
{
if( !spiCoord_AT(((y+n)*nCols)+(x+m)) )
{

spiCoord[(tarSpiCOUNT*2)+0] = (x+m);
spiCoord[(tarSpiCOUNT*2)+1] = (y+n);
spiCoord_AT(((y+n)*nCols)+(x+m)] = 1;

pt_temp.x = (x+m);
pt_temp.y = (y+n);
holds.push(pt_temp);

prevTarX = spiCoord[(tarSpiCOUNT*2)+0];
prevTarY = spiCoord[(tarSpiCOUNT*2)+1];

tarWinCOUNT++;
tarSpiCOUNT++;
tarTotCOUNT++;

}
}
}
}
if(tarWinCOUNT > 0)
{
holds.pop();
prevTarX = spiCoord[((tarSpiCOUNT-1)*2)+0];
prevTarY = spiCoord[((tarSpiCOUNT-1)*2)+1];
}
}

f64 xTOT=0;
f64 yTOT=0;
f64 xAVG=0;
f64 yAVG=0;

f32 zMAX=0;
f32 zTemp;

if( tarSpiCOUNT >= minRegSize )
{

zMAX = -99999.00;

for( uint32 w=0; w<tarSpiCOUNT; w++)
{

x = spiCoord[(w*2)+0];
y = spiCoord[(w*2)+1];
xCoord = xMin + ( x * xDim );
yCoord = yMax - ( y * yDim );
xTOT += xCoord;
yTOT += yCoord;

zTemp = ras_hi->get_rasDatCoord_f(xCoord, yCoord, 0);

if(zTemp > zMAX)
zMAX = zTemp;

}
}
```

```

xAVG = xTOT / tarSpiCOUNT;
yAVG = yTOT / tarSpiCOUNT;

if( (xAVG >= xMinCl) && (xAVG < xMaxCl) && (yAVG >= yMinCl) && (yAVG < yMaxCl) )
{
  if(TARGET == 25)
    fprintf(fp, "%d, %.2f, %.2f, %.2f, %.2f, %d\n", gtRegCOUNT, xAVG, yAVG, zMAX, tarSpiCOUNT*xDim*yDim, TARGET);
  else if( (TARGET == 2) && (tarSpiCOUNT < 200) )
    fprintf(fp, "%d, %.2f, %.2f, %.2f, %.2f, %d\n", gtRegCOUNT, xAVG, yAVG, zMAX, tarSpiCOUNT*xDim*yDim, TARGET);
  gtRegCOUNT++;
}
}

tarSpiCOUNT = 0;

}
}
}

}
}

```

“awk.distance” is the AWK program to process the output data, above. It reads in all of the data and removes some of the points collected in the 2nd pass.

```

BEGIN {

  FS=",";

  aCOUNT = 0;
  bCOUNT = 0;

  minDIST = 1.3;

  if(oFile=="") oFile="file.txt";

  if(xMin=="") exit(1);
  if(xMax=="") exit(1);
  if(yMin=="") exit(1);
  if(yMax=="") exit(1);

  if(nRegs=="") exit(1);

  regSize = ((xMax - xMin) / nRegs);

  for(b=0; b < nRegs; b++)
  {
    for(a=0; a < nRegs; a++)
    {
      accounts[a,b] = 0;
      bcounts[a,b] = 0;
    }
  }

}

NR > 1 {

  x = $2;
  y = $3;

  xLoc = int( (x - xMin) / regSize );
  yLoc = int( (y - yMin) / regSize );

```

```
if($6 == 25)
{
    anum=accounts[xLoc,yLoc];

    adata[xLoc,yLoc,anum,0] = $1;
    adata[xLoc,yLoc,anum,1] = $2;
    adata[xLoc,yLoc,anum,2] = $3;
    adata[xLoc,yLoc,anum,3] = $4;
    adata[xLoc,yLoc,anum,4] = $5;

    accounts[xLoc,yLoc]++;

}
else
{
    bnum=bcounts[xLoc,yLoc];

    bdata[xLoc,yLoc,bnum,0] = $1;
    bdata[xLoc,yLoc,bnum,1] = $2;
    bdata[xLoc,yLoc,bnum,2] = $3;
    bdata[xLoc,yLoc,bnum,3] = $4;
    bdata[xLoc,yLoc,bnum,4] = $5;
    bdata[xLoc,yLoc,bnum,5] = 0;

    bcounts[xLoc,yLoc]++;

}
}

END {

    find_deletes3();

    write_file();

}

function find_deletes3()
{
    for(a=0; a<nRegs; a++)
    {
        for(b=0; b<nRegs; b++)
        {

            anum=accounts[a,b];
            bnum=bcounts[a,b];

            for(m=0; m<anum; m++)
            {

                x1 = adata[a,b,m,1];
                y1 = adata[a,b,m,2];

                for(n=0; n<bnum; n++)
                {

                    if( !bdata[a,b,n,5] )
                    {

                        x2 = bdata[a,b,n,1];
```

```
        y2 = bdata[a,b,n,2];

        dist = sqrt((x1-x2)^2 + (y1-y2)^2);

        if(dist < minDIST)
        {
            bdata[a,b,n,5] = 1;
        }
    }
}
}
}

function write_file()
{

    printf("%5s,%12s,%12s,%9s,%9s,%9s\n", "id", "x", "y", "height", "area", "class") > oFile;

    for(a=0; a<nRegs; a++)
    {
        for(b=0; b<nRegs; b++)
        {

            anum=accounts[a,b];
            bnum=bcounts[a,b];

            for(m=0; m<anum; m++)
            {
                printf("%5d,%12.2f,%12.2f,%9.2f,%9.2f,%9d\n", adata[a,b,m,0], adata[a,b,m,1], adata[a,b,m,2], adata[a,b,m,3], adata[a,b,m,4], "25") >
oFile;
            }
            for(n=0; n<bnum; n++)
            {
                if(!bdata[a,b,n,5])
                    printf("%5d,%12.2f,%12.2f,%9.2f,%9.2f,%9d\n", bdata[a,b,n,0], bdata[a,b,n,1], bdata[a,b,n,2], bdata[a,b,n,3], bdata[a,b,n,4], "2") >
oFile;
                else
                    printf("%5d,%12.2f,%12.2f,%9.2f,%9.2f,%9d\n", bdata[a,b,n,0], bdata[a,b,n,1], bdata[a,b,n,2], bdata[a,b,n,3], bdata[a,b,n,4], "2") >
oFile"_del";
            }

        }
    }
}
}
```

References

- [1] K. I. Bang, "Alternative Methodologies for Lidar System Calibration" Ph.D. Dissertation, University of Calgary, Calgary, 2010.
- [2] T. Schenk, "Modeling and Analyzing Systematic Errors in Airborne Laser Scanners" Ohio State University, Columbus, 2001.
- [3] C. Toth, "Calibrating airborne Lidar systems" in *ISPRS Commission II Symposium*, Xi'an, 2002.
- [4] A. Wehr, "Lidar Systems and Calibration" in *Topographic Laser Ranging and Scanning*, Boca Raton, FL: CRC Press, Taylor and Francis Group LLC, 2009, pp. 129-172.
- [5] A. M. A. W. Group, "ASPRS Positional Accuracy Standards for Digital Geospatial Data" American Society for Photogrammetry and Remote Sensing, 2014.
- [6] J. R. McAuliffe, E. P. Hammerlynck and M. C. Eppes, "Landscape dynamics fostering the development and persistence of long-lived creosotebush (*larrea tridentata*) clones in the Mojave Desert" *Journal of Arid Environments*, vol. 69, pp. 96-126, 2007.
- [7] E. P. Hammerlynck, J. R. McAuliffe, E. V. McDonald and S. D. Smith, "Impacts of desert soil processes and drought on contrasting Mojave Desert shrubs" *Ecology*, vol. 83, pp. 768-779, 2002.
- [8] W. H. Schlesinger, J. F. Reynolds, G. L. Cunningham, L. F. Huenneke, W. M. Jarrell, R. A. Virginia and W. G. Whitford, "Biological feedbacks in global desertification" *Science*, vol. 247, no. 4946, pp. 1043-1048, 1990.
- [9] W. H. Schlesinger, A. E. Hartley and J. A. Raikes, "On the spatial pattern of soil nutrients in desert ecosystems" *Ecology*, vol. 77, pp. 364-374, 1996.
- [10] L. Ridolfi, F. Laio and P. D'Odorico, "Fertility island formation and evolution in dryland ecosystems" *Ecology and Society*, vol. 13, no. 1, 2008.
- [11] E. L. Mudrak, J. L. Schafer and A. Fuentes-Ramirez, "Predictive modeling of spatial patterns of soil nutrients related to fertility islands" *Landscape Ecology*, vol. 29, pp. 491-505, 2014.
- [12] R. Meyer, "U.S. Department of Agriculture, Forest Service" 2008. [Online]. Available: <http://www.fs.fed.us/database/feis/animals/reptile/goag/all.html>. [Accessed 08 January 2015].

- [13] R. B. Bury, J. D. Germano, R. T. Van Devender and R. M. Thomas, "The desert tortoise in Mexico" in *The Sonoran Desert Tortoise*, R. T. Van Devender, Ed., Tucson, AZ: The University of Arizona Press, 2002, pp. 86-108.
- [14] D. A. Walde, L. M. Harless, K. D. Delaney and L. L. Pater, "Anthropogenic threat to the desert tortoise (*Gopherus agassizii*): litter in the Mojave Desert" *Western North American Naturalist*, vol. 67, no. 1, pp. 147-149, 2007.
- [15] D. Caldwell, "Revised Recovery Plan for the Mojave Population of the Desert Tortoise" Federal Register, Sacramento, 2011.
- [16] K. Saylam, "Quality assurance of lidar systems: mission planning" in *American Society of Photogrammetry and Remote Sensing Conference*, Baltimore, MD, 2009.